International Journal of Pharmaceutics 602 (2021) 120547

Contents lists available at ScienceDirect

International Journal of Pharmaceutics

journal homepage: www.elsevier.com/locate/ijpharm

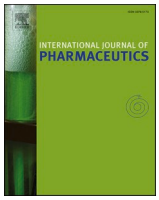

Effect of air pockets in drug delivery via jet injections

Pankaj Rohilla, Emil Khusnatdinov, Jeremy Marston *

Department of Chemical Engineering, Texas Tech University, Lubbock, TX 79409, United States

ARTICLE INFO

Keywords:
Jet
Injector
Intradermal
Viscosity
Bubble

ABSTRACT

Needle-free jet injections are actuated by a pressure impulse that can be delivered by different mechanisms to generate high-speed jets ($V_j \sim \mathcal{O}(10^2)$ m/s). During filling and transportation of disposable cartridges and ampoules, bubbles can form, which can be problematic especially for viscous fluids. Here, we report on the effect of location and size of entrapped air pockets in cartridges used in spring-powered jet injections. As air bubbles pass through the orifice, they undergo depressurization, which results in intermittent atomization and spray formation, temporarily increasing the jet dispersion. Atomization and dispersion of the jet can lead to product loss during an injection. We find that the effect of bubble location on the jet exit speed, delivery efficiency, and the projected area of the blebs formed after the injection was statistically significant ($p < 0.05$). The findings of this study have implications for the development of pre-filled cartridges for jet injection applications.

1. Introduction

Conventional oral administration of drugs is limited by low bioavailability caused by the acidic environment in the stomach and restrictive intestinal epithelium (Prausnitz et al., 2004). The most common alternatives to oral drug delivery are hypodermic needle syringes, which have numerous caveats including needle-stick injuries, cross-contamination, and needle-phobia (Weniger and Mark, 1200; Elisabetta et al., 2005; Jacobson et al., 2001) and potential limitation on injectability of viscous drugs. Thus, evidently there is a need for an effective needle-free technique for drug administration. Needle-free jet injectors are one such approach are one such example where a high-speed jet (velocity, $v_j \sim 100$ m/s; diameter, $d_j \sim 100$–200 μm) punctures the top layer of the skin (*i.e. stratum corneum*) and deposits the drug into the intradermal, subcutaneous, or intramuscular tissue (Schramm-Baxter and Mitragotri, 2004).

Medical devices such as hypodermic syringes and needle-free jet injectors need an ampoule or cartridge to store medication or biological drugs before injection. These are either supplied prefilled or can be loaded manually. Prefilled ampoules are designed to have low variability in the amount of drug (Beyea and Nicoll, 1995). However, air pockets can form in medication contained in ampoules during loading or transportation, which can be further amplified by the viscosity of the contained fluid. The effect of air pockets on the efficacy of drug delivery is still largely unknown which demands a systematic parametric study to further the current understanding.

In general, the presence of air pockets within a drug is either undesirable or could be harnessed in several medical applications (Brennen, 2014; Christopher Earls Brennen, 2015; Tang et al., 2002; Tezel et al., 2002; Tezel and Mitragotri, 2003). Ultrasound imaging (Crum et al., 2010; Blomley et al., 2001), lithotripsy (Sokolov et al., 2001), controlled cavitation in gene delivery (Blomley et al., 2001 and laser-induced jet injection Rodriguez et al., 2017; Kiyama et al., 2019; Rohilla and Marston, 2020) are some of the applications where energy generated due to the formation and collapse of air pockets can be utilized. On the other hand, the phenomenon of collapsing air pockets also generates microjets and shock waves, which can rupture red blood cells in artificial heart valves and can be detrimental to soft tissue (Garrison et al., 1994; Johansen, 2004; Rambod et al., 1999).

Introducing air bubbles (*0.1–0.2 ml*) before drawing medication into a syringe was a common-place practice among clinicians and nurses in the United States before the widespread use of disposable syringes in the 1960s (Beyea and Nicoll, 1995; Nicoll and Hesby, 2002). These air bubbles were used to correct the medication dosage to account for the dead volume in the needle hub. Moreover, air pockets when injected with the medication were thought to prevent the seepage or backflow of the medication into the subcutaneous layer through the needle tracks (Quartermaine and Taylor, 1995). However, multiple studies showed contradictory results to this hypothesis (Ipp et al., 1990; Liam, 2013). Also, air bubbles occupy the available volume for the medication which causes dosage inaccuracy (Chaplin et al., 1985). Thus, it is recommended to avoid air bubbles in syringe injections (Beyea and Nicoll,

* Corresponding author.
E-mail address: jeremy.marston@ttu.edu (J. Marston).

https://doi.org/10.1016/j.ijpharm.2021.120547
Received 3 February 2021; Received in revised form 15 March 2021; Accepted 24 March 2021
Available online 6 April 2021

1995; Nicoll and Hesby, 2002; Chaplin et al., 1985).

In jet injection, air bubbles can affect the coherency and continuity of the jet stream in addition to causing dosage errors. This phenomenon intensifies with an increase in plunger speed. Thus, in the context of jet injectors where the jet speeds can be $\mathcal{O}(10^2)$ m/s, it is important to study the effect of air pockets in the nozzle on the efficacy of jet injections. Although researchers have studied the effect of cavitation in the storage and injection of therapeutics (Brennen, 2014; Christopher Earls Brennen, 2015; Sederstrom, 2013; Theresa Trummler et al., 2020; Jean-Christophe Veilleux et al., 1068; Daou et al., 2017; Li et al., 2016; Oguri and Ando, 2018; Xiang and Wang, 2018), there is a lack of detailed study on understanding the role of air pockets in drug delivery via jet injections. Here, we study the effect of location of air pockets inside the nozzle cartridge on the hydrodynamics and efficacy of drug delivery via jet injection. The physical properties of the liquid and nozzle dimensions were kept constant. We study the bubble dynamics including atomization of the bubble within the nozzle and the dispersion of the jet when bubbles exit through the orifice. A limited ex-vivo study was conducted on porcine skin to understand the effect of air pockets on the delivery efficiency via jet injections.

2. Materials and methods

A spring-based jet injector (*Bioject ID pen*) was used in the experiments, which is described in detail in other works (Rohilla et al., 2019; Rohilla and Marston, 2019; Rohilla et al., 2020). DI water was filled in a transparent nozzle cartridge with a volume capacity of 0.11 ml and an orifice exit diameter $d_o \sim 157\ \mu m$. Air pockets were introduced at different locations inside the nozzle cartridge (as shown in Fig. 1(a,b)) using 1 ml luer-lock syringe equipped with a 24-gauge needle. Furthermore, the plunger was carefully replaced to avoid the escape of air pockets through the orifice exit. We have used five different locations within the nozzle cartridge to understand their effect on the bubble dynamics with time, chosen to cover a range of locations that can be reproduced by injection with a needle. L_1 represents the location of an air pocket at or in close proximity of the plunger tip. Locations L_2 to L_5 refer, respectively, to bubbles located at the corner between the plunger and the cartidge wall, the corner prior to the taper, at the mout of the main taper section, and in the main cartrdieg barrel. It should also be noted that the bubble locations, L_2 and L_3 are 'corner' locations (from the side-view perspective shown), however due to the radial symmetry, the exact radial location within the cartridge does not affect the dynamics.

To capture the bubble and jet dynamics, a high-speed video camera (*Phantom V711, Vision Research Ltd.*) was used at frame rates of 10,000–30,000 frames per second. The plunger displacement was measured frame-by-frame by tracking the tip of the plunger (Fig. 1(b)) using Photron FASTCAM Analysis (PFA ver.1.4.3.0) software. The plunger speed was then estimated from the slope of the displacement–time plot after the initial ringing phase, e.g. $t > 5$ ms (Fig. 1 (c)). We then estimated the jet speed at the orifice exit, v_j (Fig. 1(d)) from plunger speed using mass conservation, assuming the liquid to be incompressible at the experimental conditions.

A single side-view perspective was sufficient to track the plunger tip. However, to visualize the bubble dynamics within the nozzle during a jet injection, we used two cameras (*second camera: Phantom Miro 311, Vision Research Ltd.*) with orthogonal views. In addition, using extension tubes with Nikon micro-nikkor 60 mm lenses, we achieved typical effective pixel sizes in a range of 10–30 $\mu m/px$.

Volume fraction was used to quantify the size of the air pockets, which is defined as the ratio of the volume occupied by an air pocket (V_b) to the total liquid volume inside a nozzle cartridge without any air pocket (V). We measured the volume fraction occupied by air pockets at different locations by weighing the liquid-filled nozzle with and without air pockets. Fig. 1(d) shows the volume fraction of air pockets introduced at different locations inside the nozzle.

To measure the force profile during the jet injection, a miniature load button cell (*Futek-LLB 350, 50 lb, FSH04000, accuracy ±0.1%*) was

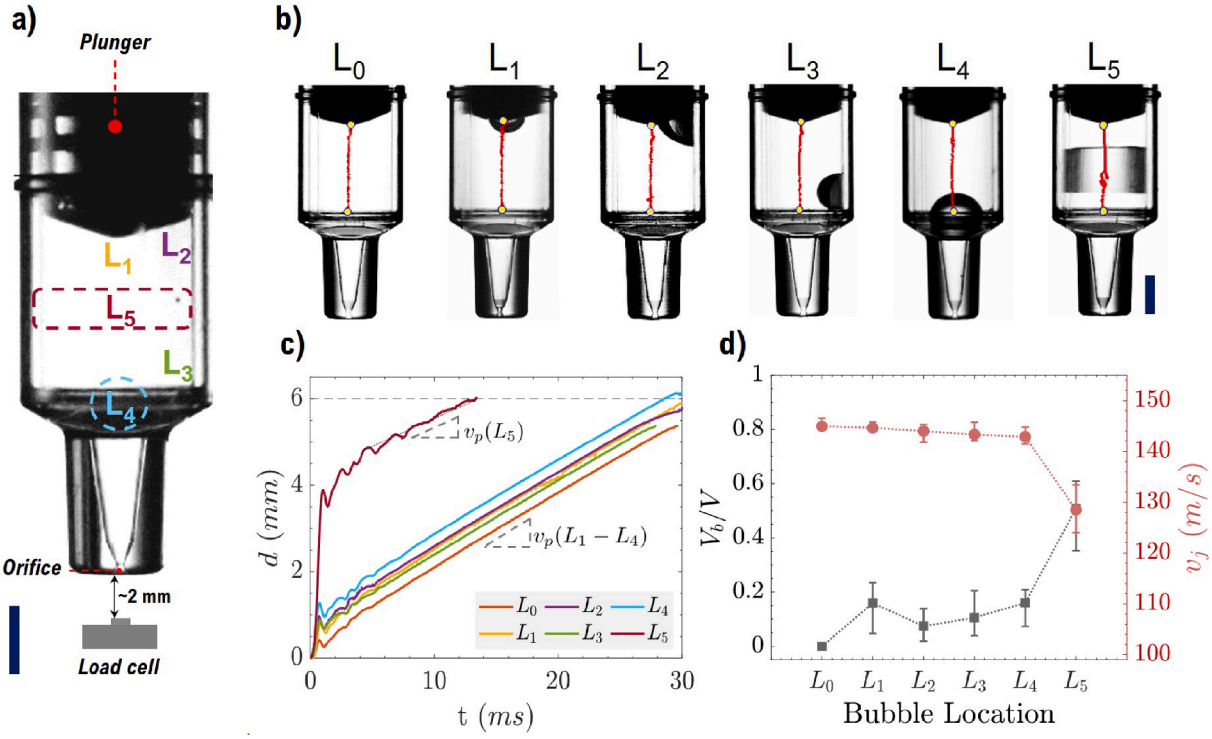

Fig. 1. Air pockets in a nozzle cartridge. (a) Five different locations of air pockets inside a nozzle cartridge, **(b)** trajectory (*in red*) of plunger motion inside the nozzle for different locations of air pockets, **(c)** plunger displacement with time for a jet injection with and without air pockets, and **(d)** volume fraction (V_b/V) and jet speed (v_j) for different locations of air pockets (n = 5, error bars represent standard deviation). Scale bar represents 3 mm (a,b).

placed at a distance of 2 mm away from the orifice exit of the nozzle to avoid contact with the nozzle (figure 1(a)) during jet injection. Force profiles of jet injection were recorded at a sample rate of 4,800 Hz.

To conduct ex vivo studies, porcine skin was used as a skin model for human skin. Porcine skin patches (*thickness* $\sim$ *3–5 mm*) were harvested from the side regions of Yorkshire-Cross pigs (age: 13 weeks), euthanized in the department of Animal Sciences (Texas Tech University). These skin patches were kept in a $-80\ ^oC$ freezer, but thawed to room temperature before jet injection. We cut skin across the center of the injection site to visualize the dispersion of the liquid after jet injection. Trypan Blue (*Sigma Aldrich*) was used as a dye (*1 mg/ml*) in DI water to aid in the visualization of skin blebs, and a custom Matlab script was used to estimate the dimensions of skin blebs. We used porcine skins after a single freeze–thaw cycle, which is generally regarded as a good model of human skin (Ranamukhaarachchi et al., 2016).

We performed one-way ANOVA tests to check the statistical significance of various parameters used in the study with a significance level of $\alpha = 0.05$.

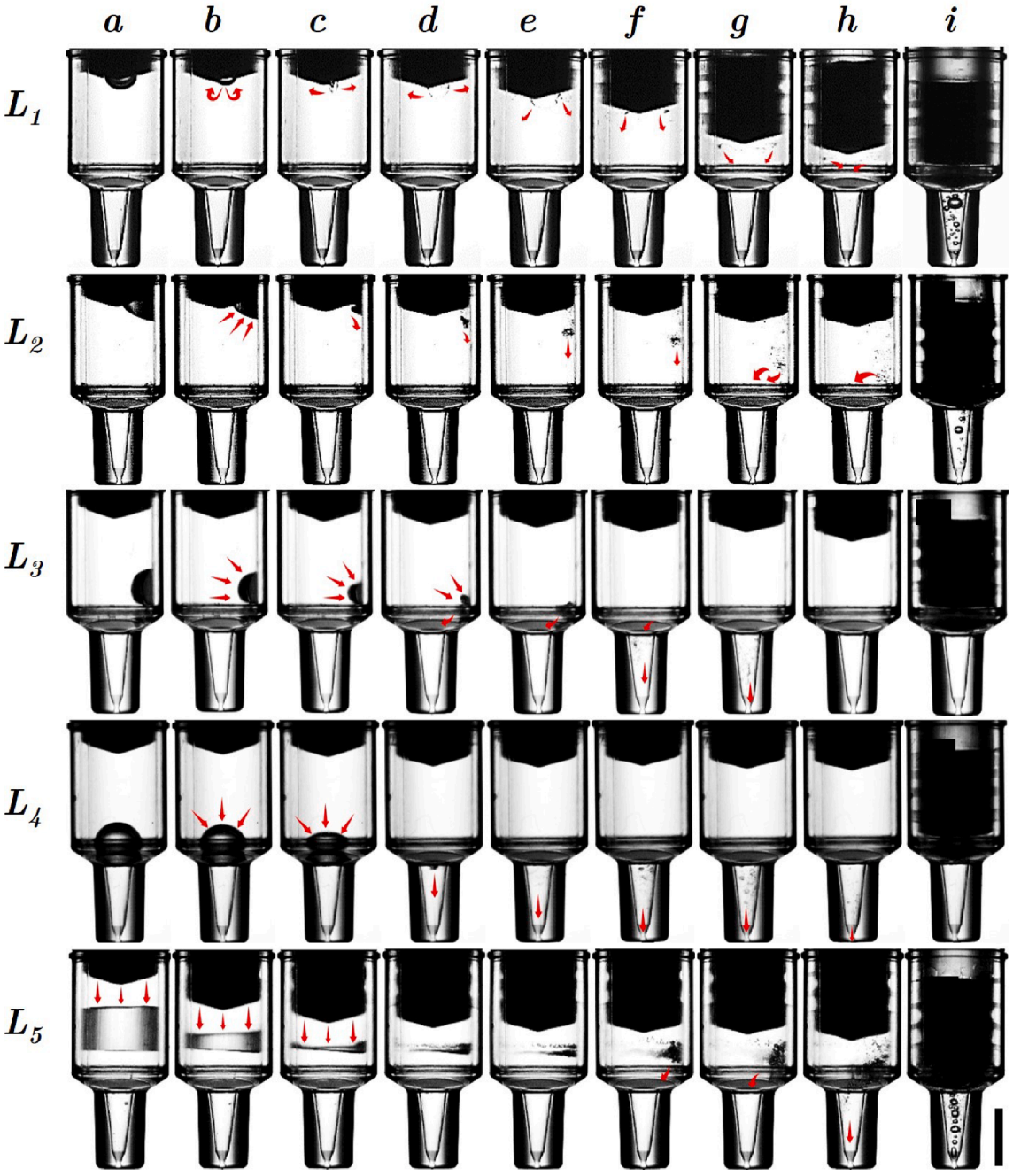

Fig. 2. Snapshots of bubble dynamics for different locations of air pockets inside the nozzle cartridge corresponding to different time frames. For location L_1, frames (a-i) $\equiv$ [0, 0.1, 0.2, 0.27, 0.37, 1.5, 2.27, 5.73, 61.07] **ms with jet ejection duration,** $t_j \sim 38$ **ms; for location** L_2**, frames (a-i)** $\equiv$ [0, 0.2, 0.3, 0.5, 1.0, 2.9, 4.57, 6.23, 61.77] **ms with** $t_j \sim 38$ **ms; for location** L_3**, frames (a-i)** $\equiv$ [0, 0.1, 0.2, 0.27, 0.37, 1.5, 2.27, 5.73, 61.07] **ms with** $t_j \sim 35$ **ms; for location** L_4**, frames (a-i)** $\equiv$ [0, 0.67, 0.167, 0.43, 0.67, 1.47, 2.23, 3.5, 64.67] **ms with** $t_j \sim 36$ **ms; and for location** L_5**, frames (a-i)** $\equiv$ [0, 0.5, 0.6, 0.67, 0.73, 1.1, 1.83, 5.3, 30.33] **ms with** $t_j \sim 17$ **ms.**

3. Results and discussions

3.1. Bubble Dynamics

Jet injection was actuated with a trigger, which initiated the decompression of the spring causing the plunger to move instantaneously. The impact of the plunger causes rapid pressurization and the air bubble atomizes into multiple microbubbles, whilst the ensuing plunger motion forces the liquid out through a narrow orifice exit (157 μm). Fig. 1(c) shows the plunger motion, which exhibits a 'ringing' (oscillatory) phase caused by the sudden impact of the spring piston on the plunger, followed by a nearly linear and stable motion. Average jet speeds were calculated from the slope of this linear region of the plunger displacement–time plot. Introduction of air pockets did not alter the steady jet speed (v_j) significantly which lied in a range of $\sim$ 142–146 m/s, except for the case of air pocket introduced at the center of the nozzle cartridge (L_5).

Among the different locations of air pockets, L_5 showed a distinctive behavior. The plunger moved $\sim$ 3.7 mm through the cartridge barrel within a short period of 1.5 ms, thus resulting in a rapid collapse of the air pocket. The collapsing air pocket generates a pressure opposing the plunger motion, and the interplay of forces during this period is manifested by the recoiling trajectory of the plunger, as shown in the last frame of Fig. 1(b). The impulse is much stronger, and resistance in the early stages is much weaker, leading to significant over-pressure (noted by a force increase of $\sim$ 33%). This resulted in a higher initial jet speed, but also a prolonged recoil/ringing phase. Due to this extended ringing phase, we calculated the average jet speed by fitting a line after this phase to the plunger displacement–time plot. For L_5, average jet speed was lower (128.5 $\pm$ 3.8 m/s). Another important characteristic of air pockets introduced at different locations inside the nozzle was the volume fraction of the air pocket. For locations L_1 –L_4, the volume fraction occupied by the air pocket was in the range of $\sim$ 5–25%. However, the volume fraction of the air pocket at location L_5 was in the range $\sim$ 40–60%. A larger air bubble was required for the center location in order to stabilize it at that location; volumes smaller than this range tended to move to locations L_1 –L_4.

Fig. 2 shows a montage of frames summarizing the bubble dynamics for air pockets placed at different locations. When the plunger is triggered, the fluid pressure in the cartridge increases rapidly up to $\mathcal{O}$(10 MPa), causing the air pocket to collapse and disintegrate into microbubbles. The trajectory of such microbubbles largely depends on the pressure gradient, which further depends on the flow disturbance caused by the bubbles collapsing under high pressure. Although numerous studies have been conducted to understand the behavior of bubbles with inertial impact (Daou et al., 2017; Li et al., 2016; Rodríguez-Rodríguez et al., 2014), the underlying physics behind the bubble dynamics may vary on the basis of applications.

The life cycle of microbubbles depends on the location where the air pocket was introduced initially. For air pockets present near the outlet (L_3 and L_4), microbubbles exit the nozzle at an early stage whereas for air pockets introduced farther upstream, not all of these bubbles exit; it can be noticed from i^{th} frames in Fig. 2 that microbubbles were present in the tapered section of the nozzle at the end of injection for air pocket introduced at locations L_1,L_2, and L_5.

Fig. 3 shows orthogonal views of microbubbles inside the nozzle at the same instant (t = 5.5 ms). Different views shown in Fig. 3 yield different bubble size distributions at the same instant of time due to the lensing effects of the nozzle geometry. Thus, to avoid the erroneous measurement, we did not quantify the bubble size distribution with time.

Assuming the air bubble to be an ideal gas, we can estimate the volume of the wedge-shaped bubble cloud formed after the collapse of an air pocket at location L_5, using ideal gas law ($PV = nRT = const.$):

$$P_1 V_1 = P_2 V_2 \tag{1}$$

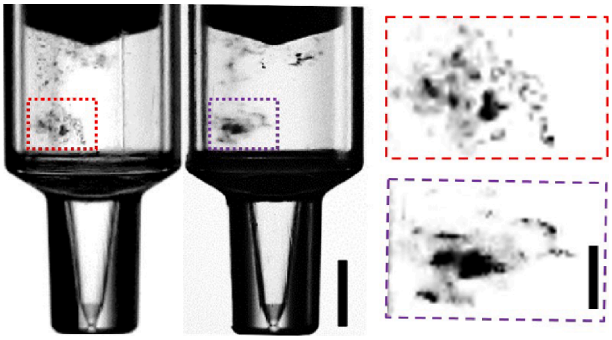

Fig. 3. Orthogonal views of nozzle cartridge with microbubbles inside the liquid corresponding to time, t = 5.5 ms for air pocket introduced at location L_2. *Scale bar represents 3 mm.* **Note:** A vertical line on the left frame is an artifact of the nozzle and is not related to the contained fluid or air pockets.

Where P_1 and P_2 are atmospheric pressure ($\sim 10^5$ Pa) and pressure inside the bubble ($\sim 5\times10^7$ Pa, using peak force of $F^* \sim 1$ N), respectively. V_1 and V_2 are the initial volume of the air pocket ($\sim$ 55 μL, for location L_5) and the volume of the wedge-shape bubble cloud after the collapse, respectively. The minimum height of the bubble cloud (h_{min}) was estimated using:

$$h_{min} \approx \frac{V_2}{\left(\pi \frac{D_i^2}{4}\right)} \tag{2}$$

Where D_i is the inner diameter of the nozzle barrel.

A slight asymmetry in the shape of the air pocket (L_5) causes a wedge-shaped air volume that disintegrates from left to right in the image sequence (see Fig. 2, L_5(*a-i*)), therefore, we can expect a size distribution with $r_{min} \ll 10$ μm and $r_{max} \gg 10$ μm, evidenced by zoomed images where bubbles with size of $\mathcal{O}$(100 μm) can be easily seen. Moreover, many bubbles with a size of the order of 1 pixel or less were also observed, in agreement with our quantitative argument.

3.2. Force measurements

To measure the impact force, liquid jets were impinged on a load cell placed at a distance of 2 mm away from the orifice exit. Fig. 4 shows force profiles of jets with air pockets present at different locations. The time duration of the jets for air pocket locations L_1, L_2, L_3, L_4 and L_5 were $\sim$ 37.5 ms, $\sim$ 34.8 ms, $\sim$ 35.8 ms, $\sim$ 33.5 ms, and $\sim$ 16.9 ms, respectively. In the absence of an air pocket, the time duration of a water jet was $\sim$ 38 ms. Force profiles are more reliable for determining the jet duration compared to displacement profiles due to the difficulties associated with tracking the plunger tip towards the end of injection.

As the spring piston strikes the plunger, a ringing phase can be observed in force profiles in the initial stage ($\sim$ 10 ms) of liquid injection. In the absence of any air pockets, the peak force was $\sim$ 0.63 N and a similar peak force was observed for air pockets present at locations L_1, L_2, L_3, and L_4 with values of $\sim$ 0.62 N, $\sim$ 0.76 N, $\sim$ 0.67 N, and $\sim$ 0.78 N, respectively. However, L_5 exhibited a higher force of $\sim$ 1.03 N, representing an increase of 63% compared to the other locations. After the peak force, the magnitude of the force profile was nearly the same for all cases with $\overline{F} \simeq 0.4$ N ($\overline{F} = \rho v_j^2 A_o$ (Rohilla and Marston, 2019; Uth and Deshpande, 2013), *where A_o is the cross-sectional area of orifice exit*) except the case of L_5 with slightly lower force. Further implications of force profile and injection duration will be discussed in ex vivo studies.

3.3. Effect of microbubbles on jet collimation

As pressurized microbubbles exit the orifice, they undergo a rapid depressurization and expand, resulting in a spray-like jet (Fig. 5). The

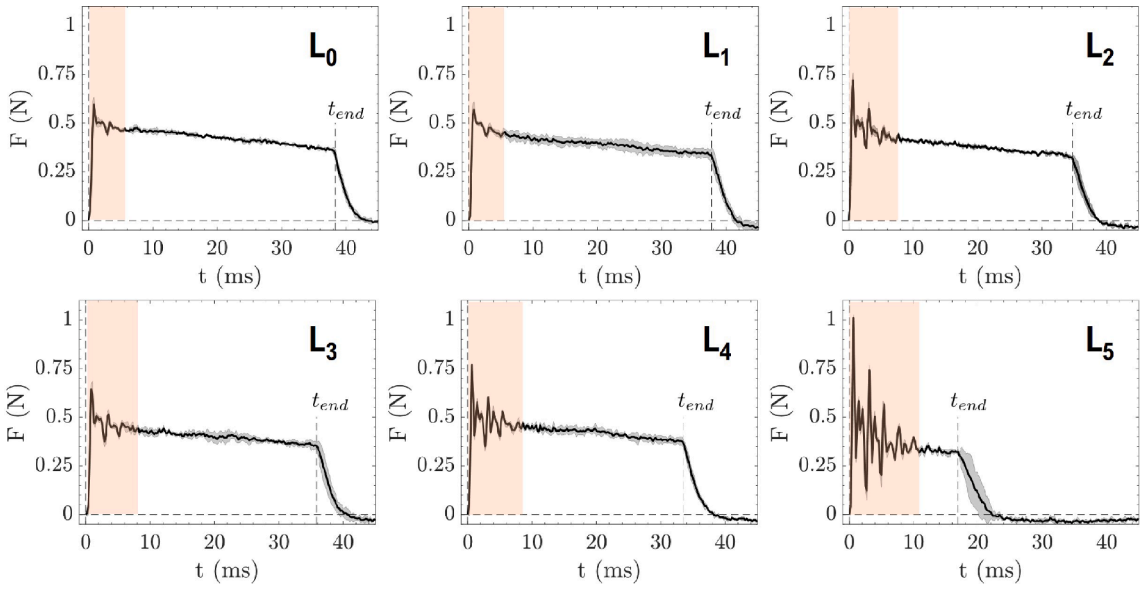

Fig. 4. Impact force profiles for jet injections for different locations of air pockets. L_0 represents the jet injection without any air pocket inside the nozzle. Shaded region represents ringing phase during jet injection. (*n = 3, shaded error bars represent standard deviation*).

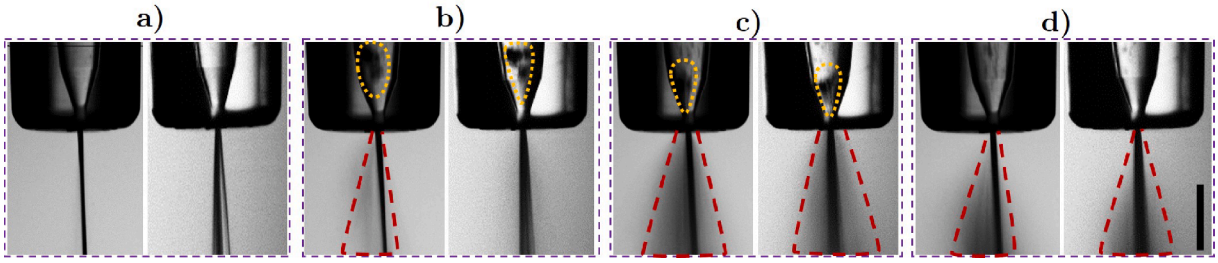

Fig. 5. Effect of bubbles on the jet coherency with orthogonal views. (a). liquid jet without any bubbles ($t = 1.4$ *ms*), (b) bubble cloud in tapered section before exit (t = 9.9 ms), (c) spray-like jet formation as the bubbles exit with the jet (t = 10 ms), and (d) diminishing atomization of jet as bubble clouds exits the tapered section (t = 10.1 ms). Yellow outlines show a cloud of micro-air bubbles within the tapering section of the nozzle and the red outlines show the spray formation as the microbubbles exit the orifice. The scale bar in panel (d) represents 2 mm.

magnitude of the effect of microbubbles on the jet depends on the size and the number of bubbles exiting the nozzle orifice along the liquid jet.

Fig. 5 shows the effect of a bubble cloud exiting the nozzle orifice on the liquid jet with orthogonal views captured using two high-speed cameras at a frame rate of 10,000 fps. The liquid jet free of any effect of bubbles is shown in Fig. 5(a), where orthogonal views show that the jet looks coherent from one side and slightly dispersed from the other side. In the next frame (Fig. 5(b)), a cloud of air pockets (*highlighted in dashed yellow outlines*) appeared in the tapered section of the nozzle with spray-like jets as the bubbles exit with the jet. As more bubble clouds exit the nozzle, the jet dispersion grows as shown in Fig. 5(c). With the majority of air pockets exiting the orifice exit, the remnant effects of the bubbles on the liquid jet can be seen in Fig. 5(d), but the jet will resume the steady stream upon clearance of air bubbles.

3.4. Ex vivo studies

To understand the effect of air pockets in injection into real tissue, we performed jet injection of dyed water into porcine skin, which was harvested from different pigs at the department of Animal Sciences (hence, different colors in Fig. 6). In previous studies (Rohilla et al., 2020) the effect of force exerted by the jet injector in the normal direction (i.e. *loading*) has been reported, and therefore we used the recommended normal load of 1 kg on the jet injector.

After impingement, the liquid jet creates a hole in the skin through

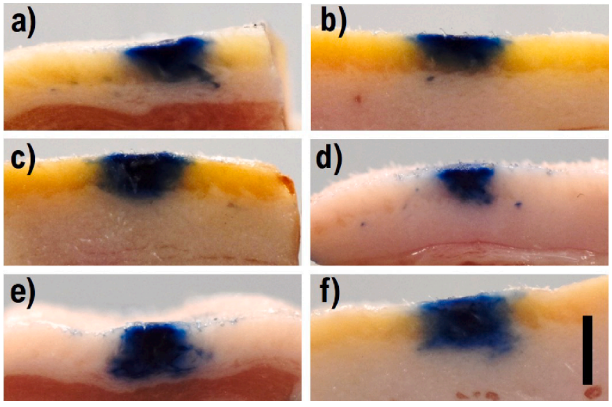

Fig. 6. Cross section view of skin blebs for: (a). no air pockets, **(b)** air pocket at location L_1, **(c)** air pocket at location L_2, **(d)** air pocket at location L_3, **(e)** air pocket at location L_4 and **(f)** air pocket at location L_5. *Scale bar represents 5 mm.*

which liquid propagates inside the skin. The stiff poro-elastic structure of the dermal tissue resists the liquid inflow inside the skin, thus limiting the amount of liquid that can be delivered with a single injection. To visualize the dispersion of liquid inside skin after jet injection, the skins were cut across the point of injection. Fig. 6 shows cross-sections of skin

blebs corresponding to the different location of air pockets. It can be seen from the cross-sectional view of the blebs that the injections were largely limited to the dermis layer, even for location L_5, which imparts a higher peak force; in that case we do see some liquid penetration into the subcutaneous tissue. In contrast, Fig. 6(d) exhibits shallow penetration and lower horizontal dispersion of liquid, which corresponds to lower delivery efficiency for air pockets at location L_3. Thus, cross-sectional views of skin blebs provide visual insights into the injection process.

Fig. 7 shows the effect of the location of the air pocket on the delivery efficiency and the dimensions of the bleb formed inside the skin after jet injection. Delivery efficiency ($\eta = (m - m_r) \times 100/m$) was measured from the weight of liquid rejected at the top of the skin after injection (m_r) and total weight of liquid in the nozzle cartridge before injection (m). Whatman filter papers were used to absorb the rejected liquid on the top of skin.

The presence of air pockets at locations L_1,L_2, and L_5 showed higher percentage delivery of liquid inside the skin, and indeed the effect of varying the location of air pockets on the delivery efficiency of dyed water was significant ($p < 0.05$). It is noteworthy that the delivery efficiency was affected by the confluence of changing location and available liquid volume inside the nozzle. As discussed earlier, the volume of liquid inside the nozzle changes with introduction of air pockets inside the nozzle. Introducing an air pocket at location L_1 showed higher percentage delivery than the case of no air pockets for nearly the same force profile. This increase in delivery efficiency could be due to the reduced liquid volume to be injected inside the skin; As shown in earlier studies (Rohilla et al., 2020), higher delivery efficiency in jet injection was obtained for lower volumes. It was hypothesized that there is a limit of liquid volume which can be injected into the skin without significant rejection. Here, with the introduction of air pockets, the available liquid volume to be injected was lower for locations L_1 and L_5, resulting in higher efficiency.

In addition, the percentage delivery was nearly the same for locations L_3 and L_4 as compared to the control case, L_0. Bubbles exit early with a jet for air pockets present at locations L_3 and L_4. As the high-speed liquid jet penetrates the skin, it creates a channel to facilitate the further delivery of incoming liquid. Any disturbance in the jet shape in the initial phase could have an adverse effect on the channel formation in the tissue for liquid propagation, thus resulting in lower percentage delivery and narrow dispersion patterns, as observed for L_3 and L_4. Higher peak force also helps in increasing percentage delivery, as noted with location L_5; We postulate that this is a confluence of the higher initial impact force ($\sim$ 1.03 N) and lower volume of liquid to be injected ($\sim$ 0.05 ml).

The effect of location of air pockets was significant on the projected area ($p < 0.05$) and the aspect ratio of skin blebs ($p < 0.05$). Projected area showed nearly the same trend as of delivery efficiency. In the case of injection with an air pocket present near the exit (L_3 *and* L_4), skin blebs showed large intra sample variation in their shape and their dimensions.

4. Conclusions

We investigated the effect of introducing air pockets at various locations within the liquid contained in a nozzle cartridge for jet injectors. When the spring-piston impacts the plunger of the cartridge, rapid pressurization causes the air pocket to collapse into microbubbles, which ultimately result in atomization as liquid exits the orifice. As such, the jet can become significantly dispersed and intermittent. The peak impact force was also affected by the presence of air pockets, whereby the largest air pocket led to the highest peak force due to a slamming phenomenon associated with the rapid collapse of the bubble. With regards to delivery, our ex-vivo measurements indicate that the delivery efficiency improved for the configuration with the largest air bubble, which we hypothesize is due to a confluence of higher initial peak velocity and reduced initial volume ($V^* \approx 50\ \mu$L), in agreement with prior reports on intradermal injections. Although this infers that introduction of air pockets can improve delivery efficiency, we postulate that air pockets should be avoided in order to eliminate dosage inaccuracy and spray via atomization, both of which could be detrimental to jet injection.

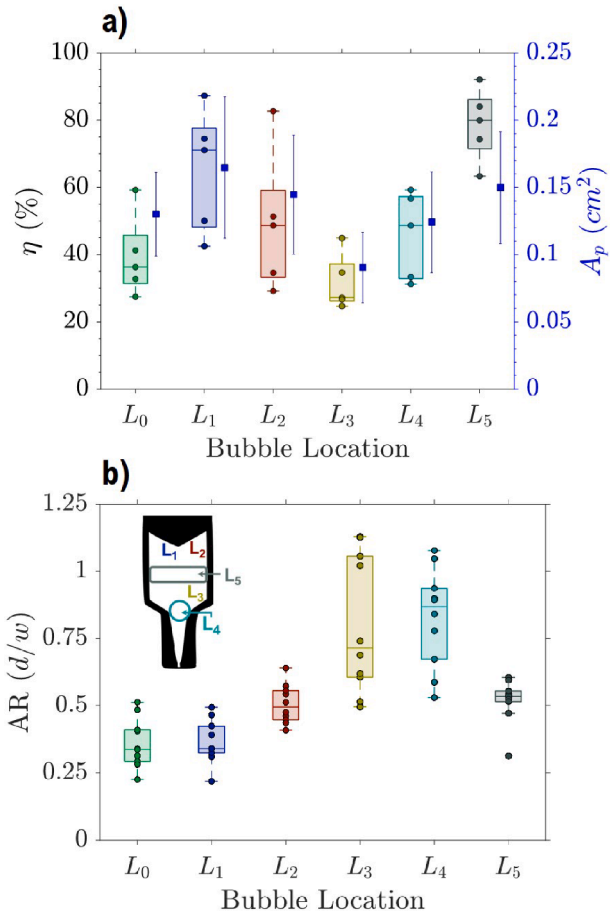

Fig. 7. Effect of air pockets on effectiveness of drug delivery. (a) delivery efficiency and projected area of bleb cross-sections for jet injections with air pockets at different locations ($n = 5$, *error bars for* A_p *represent standard deviation*) and **(b)** aspect ratio of the blebs ($AR = d/w$), where d and w are depth and width of skin bleb respectively (n = 10).

Author contributions

P. Rohilla: Methodology, Data curation, Formal analysis, Writing - original draft, Writing - final draft. **E. Khusnatdinov:** Data curation. **J. Marston:** Conceptualization, Methodology, Funding Acquisition, Writing - final draft.

Declaration of Competing Interest

The authors declare that they have no known competing financial interests or personal relationships that could have appeared to influence the work reported in this paper.

Acknowledgments

This work was financially supported by The National Science Foundation via the award CBET-1749382. We also thank Inovio Pharmaceuticals for providing the jet injector device.

Appendix A. Supplementary material

Supplementary data associated with this article can be found, in the online version, at https://doi.org/10.1016/j.ijpharm.2021.120547.

References

Beyea, Suzanne C., Nicoll, Leslie H, 1995. Administration of medications via the intramuscular route: an integrative review of the literature and research-based protocol for the procedure. Appl. Nurs. Res. 8 (1), 23–33.

Blomley, Martin J.K., Cooke, Jennifer C., Unger, Evan C., Monaghan, Mark J., Cosgrove, David O., 2001. Microbubble contrast agents: a new era in ultrasound. Bmj 322 (7296), 1222–1225.

Christopher E Brennen. Cavitation and bubble dynamics. Cambridge University Press, 2014.

Chaplin, Gail, Shull, Harriet, Welk III, Pual C, 1985. How safe is the: Air-bubble technique. Nursing 15 (9), 59–62.

Christopher Earls Brennen. Cavitation in medicine. Interface focus, 5(5):20150022, 2015.

Crum, Lawrence, Bailey, Michael, Hwang, Joo Ha, Khokhlova, Vera, Sapozhnikov, Oleg, 2010. Therapeutic ultrasound: Recent trends and future perspectives. Physics Procedia 3 (1), 25–34.

Maya Mounir Daou, Elena Igualada, Hugo Dutilleul, Jean-Marie Citerne, Javier Rodríguez-Rodríguez, Stéphane Zaleski, and Daniel Fuster. Investigation of the collapse of bubbles after the impact of a piston on a liquid free surface. AIChE Journal, 63(6):2483–2495, 2017.

Elisabetta Rapiti, A Pruss-Ustrun, and Y Hutin. Sharps injuries: Global burden of disease from sharps injuries to health-care workers. World Health Organization, Geneva, 2005.

Garrison, L.A., Lamson, T.C., Steven Deutsch, D.B., Geselowitz, R.P Gaumond, Tarbell, J. M., 1994. An in-vitro investigation of prosthetic heart valve cavitation in blood. The Journal of heart valve disease 3, S8–22.

Ipp, M., Goldbach, M., Greenberg, S., Gold, R., 1990. Effect of needle change and air bubble in syringe on minor adverse reactions associated with diphtheria-tetanus toxoids-pertussis-polio vaccination in infants. 9 (4), 291–293. The Pediatric infectious disease journal</hi>.

Robert M Jacobson, Avril Swan, Adedunni Adegbenro, Sarah L Ludington, Peter C Wollan, Gregory A Poland, Vaccine Research Group, et al. Making vaccines more acceptable methods to prevent and minimize pain and other common adverse events associated with vaccines. Vaccine, 19(17-19):2418–2427, 2001.

Jean-Christophe Veilleux, Kazuki Maeda, Tim Colonius, and Joseph E Shepherd. Transient cavitation in pre-filled syringes during autoinjector actuation. Proceedings of the 10th International Symposium on Cavitation (CAV2018), page 1068, 2018.

Johansen, Peter, 2004. Mechanical heart valve cavitation. Expert review of medical devices 1 (1), 95–104.

Akihito Kiyama, Nanami Endo, Sennosuke Kawamoto, Chihiro Katsuta, Kumiko Oida, Akane Tanaka, and Yoshiyuki Tagawa. Visualization of penetration of a high-speed focused microjet into gel and animal skin. Journal of Visualization, 22(3):449–457, 2019.

Liam Mac Gabhann. A comparison of two depot injection techniques. Nursing Standard (through 2013), 12(37):39, 1998.

Li, S., Han, R., Zhang, A.M., Wang, Q.X., 2016. Analysis of pressure field generated by a collapsing bubble. Ocean Eng. 117, 22–38.

Nicoll, Leslie H, Hesby, Amy, 2002. Intramuscular injection: an integrative research review and guideline for evidence-based practice. Applied nursing research 15 (3), 149–162.

Ryota Oguri and Keita Ando. Cavitation bubble nucleation induced by shock-bubble interaction in a gelatin gel. Physics of Fluids, 30(5):051904, 2018.

Prausnitz, Mark R, Mitragotri, Samir, Langer, Robert, 2004. Current status and future potential of transdermal drug delivery. Nature reviews Drug discovery 3 (2), 115–124.

Quartermaine, S., Taylor, R., 1995. A comparative study of depot injection techniques. Nursing Times 91(30):36.

Rambod, Edmond, Beizaie, Masoud, Shusser, Michael, Milo, Simcha, Gharib, Morteza, 1999. A physical model describing the mechanism for formation of gas microbubbles in patients with mitral mechanical heart valves. 27 (6), 774–792. Annals of biomedical engineering</hi>.

Ranamukhaarachchi, S.A., Lehnert, S., Ranamukhaarachchi, S.L., Sprenger, L., Schneider, T., Mansoor, I., Rai, K., Häfeli, U.O., Stoeber, B., 2016. A micromechanical comparison of human and porcine skin before and after preservation by freezing for medical device development. Scientific reports 6 (1), 1–9.

Carla Berrospe Rodríguez, Claas Willem Visser, Stefan Schlautmann, David Fernandez Rivas, and Ruben Ramos-Garcia. Toward jet injection by continuous-wave laser cavitation. Journal of biomedical optics, 22(10):105003, 2017.

Rodríguez-Rodríguez, Javier, Casado-Chacón, Almudena, Fuster, Daniel, 2014. Physics of beer tapping. Physical review letters 113 (21), 214501.

Rohilla, Pankaj, Marston, Jeremy O, 2019. In-vitro studies of jet injections. International journal of pharmaceutics 568 (118503).

Rohilla, Pankaj, Marston, Jeremy, 2020. Feasibility of laser induced jets in needle free jet injections. Int. J. Pharm. 589 (119714).

Pankaj Rohilla, Yatish S Rane, Idera Lawal, Andrew Le Blanc, Justin Davis, James B Thomas, Cormak Weeks, Whitney Tran, Paul Fisher, Kate E Broderick, et al. Characterization of jets for impulsively-started needle-free jet injectors: Influence of fluid properties. Journal of Drug Delivery Science and Technology, 53:101167, 2019.

Pankaj Rohilla, Idera Lawal, Andrew Le Blanc, Veronica O'Brien, Cormak Weeks, Whitney Tran, Yatish Rane, Emil Khusnatdinov, and Jeremy Marston. Loading effects on the performance of needle-free jet injections in different skin models. Journal of Drug Delivery Science and Technology, 60:102043, 2020.

Schramm-Baxter, Joy, Mitragotri, Samir, 2004. Needle-free jet injections: dependence of jet penetration and dispersion in the skin on jet power. J. Controlled Release 97 (3), 527–535.

Sederstrom, Donn, 2013. Cavitation in pharmaceutical manufacturing and shipping. Master's thesis. University of Denver.

Sokolov, Dahlia L., Bailey, Michael R., Crum, Lawrence A., 2001. Use of a dual-pulse lithotripter to generate a localized and intensified cavitation field. The Journal of the Acoustical Society of America 110 (3), 1685–1695.

Tang, Hu.a., Wang, Chiao Chun Joanne, Blankschtein, Daniel, Langer, Robert, 2002. An investigation of the role of cavitation in low-frequency ultrasound-mediated transdermal drug transport. Pharmaceutical research 19 (8), 1160–1169.

Tezel, Ahmet, Mitragotri, Samir, 2003. Interactions of inertial cavitation bubbles with stratum corneum lipid bilayers during low-frequency sonophoresis. Biophysical journal 85 (6), 3502–3512.

Tezel, Ahmet, Sens, Ashley, Mitragotri, Samir, 2002. Investigations of the role of cavitation in low-frequency sonophoresis using acoustic spectroscopy. Journal of pharmaceutical sciences 91 (2), 444–453.

Theresa Trummler, Spencer H. Bryngelson, Kevin Schmidmayer, Steffen J. Schmidt, Tim Colonius, and Nikolaus A. Adams. Near-surface dynamics of a gas bubble collapsing above a crevice. Journal of Fluid Mechanics, 899:A16, 2020.

Uth, Tobias, Deshpande, Vikram S, 2013. Unsteady penetration of a target by a liquid jet. Proc. Nat. Acad. Sci. 110 (50), 20028–20033.

Bruce G Weniger and Mark J Papania. Alternative vaccine delivery methods. Vaccines, page 1200, 2013.

Xiang, Gaoming, Wang, Bing, 2018. Numerical investigation on the interaction of planar shock wave with an initial ellipsoidal bubble in liquid medium. AIP Advances 8 (7), 075128.